Volume 15
Number 10
14 March 2023
Pages 1243–1388

Analytical Methods

rsc.li/methods

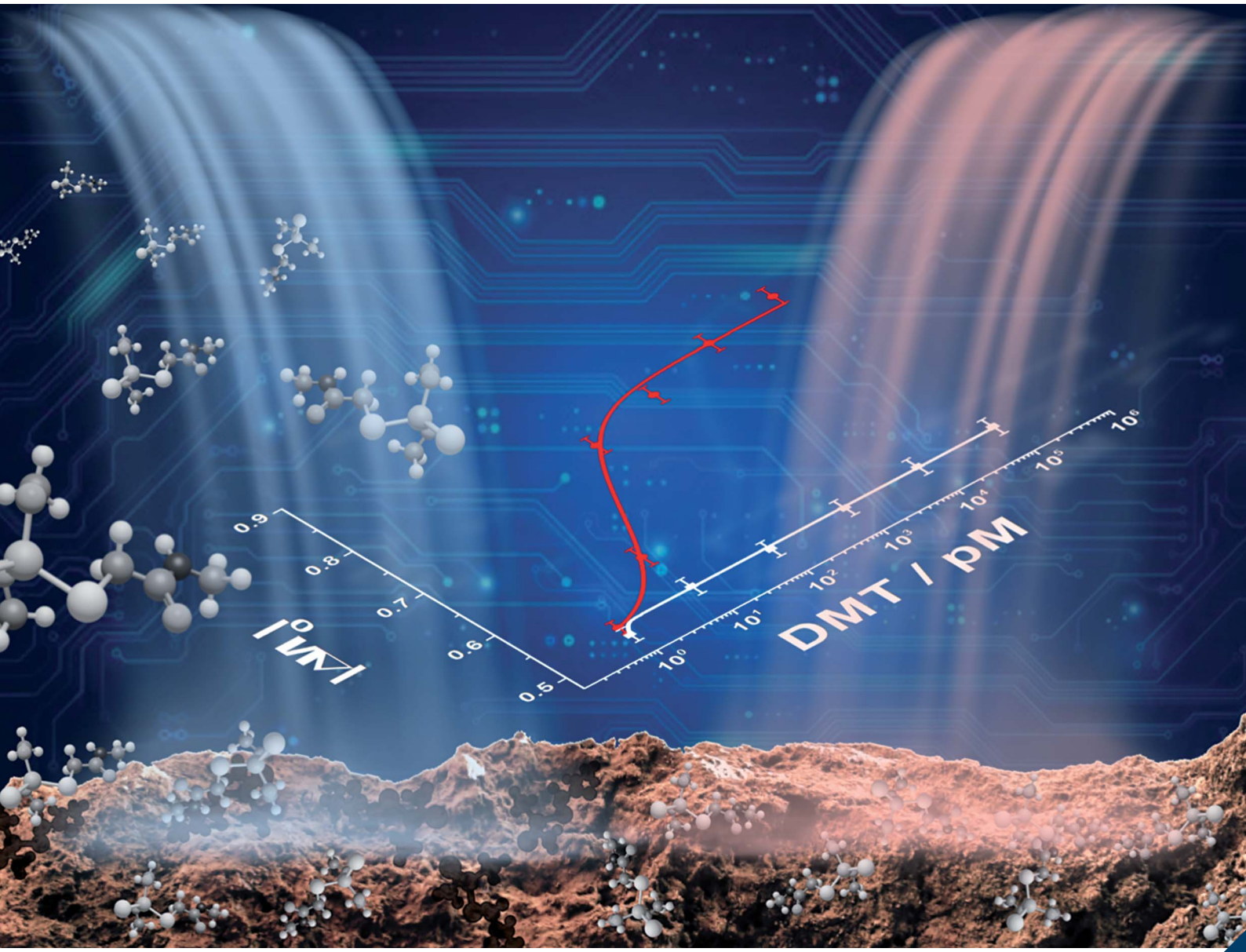

ISSN 1759-9679

ROYAL SOCIETY OF CHEMISTRY

COMMUNICATION

Paolo Bollella, Nicoletta Ditaranto *et al.*
Electropolymerized molecularly imprinted polypyrrole film for dimethoate sensing: investigation on template removal after the imprinting process

Indexed in Medline!

Analytical Methods

ROYAL SOCIETY OF CHEMISTRY

COMMUNICATION

View Article Online
View Journal | View Issue

Cite this: *Anal. Methods*, 2023, **15**, 1250

Received 15th December 2022
Accepted 20th January 2023

DOI: 10.1039/d2ay02024f

rsc.li/methods

Electropolymerized molecularly imprinted polypyrrole film for dimethoate sensing: investigation on template removal after the imprinting process†

Marlene Valentino,‡[a] Anna Imbriano,‡[b] Angelo Tricase,[ab] Flavio Della Pelle,[c] Dario Compagnone,[c] Eleonora Macchia,[de] Luisa Torsi,[abe] Paolo Bollella*[ab] and Nicoletta Ditaranto*[ab]

The development of ultrasensitive analytical detection methods for organophosphorus pesticides such as dimethoate (DMT) plays a key role in healthy food production. DMT is an inhibitor of acetylcholinesterase (AChE), which can lead to the accumulation of acetylcholine and result in symptoms related to the autonomous and central nervous systems. Herein, we report the first spectroscopic and electrochemical study on template removal after an imprinting process from a polypyrrole-based molecularly imprinted polymer (PPy-MIP) film for the detection of DMT. Several template removal procedures were tested and evaluated using X-ray photoelectron spectroscopy. The most effective procedure was achieved in 100 mM NaOH. The proposed DMT PPy-MIP sensor exhibits a limit of detection of $(8 \pm 2) \times 10^{-12}$ M.

Molecular and biomolecular recognition are widely employed for the development of sensing devices able to detect biological, food and environmental contaminants.[1–3] Recently, many molecularly imprinted polymer (MIP) modified electrodes have been developed with the inclusion of nanomaterials to increase the chemical stability of the polymer layer and its sensitivity towards analytical targets.[4] Many studies on the usage of MIPs in the selective separation and detection of chemical/biological active molecules such as proteins, amino acids and pesticides have been published in the literature in recent years.[5–10] MIPs are also used in a wide variety of applications, including sample preparation (*e.g.*, solid phase extraction), chromatographic separation, chemical sensing, and drug delivery.[11–13] With respect to bioreceptors, MIPs exhibit similar selectivity and sensitivity to antibody-modified electrodes. However, MIPs can be easily produced on demand for a plethora of analytical targets, making them cheaper than antibody modified electrodes.[14] Despite their features, several issues have been reported on the initial template removal step of MIPs considering their incomplete, as well as unclear, definition of the template removal mechanism.[15] Usually, the interactions involved in MIP electropolymerization are relatively weak, such as van der Waals interactions and hydrogen bonding.[16] Indeed, there are several studies that have discussed MIP preparation, effectiveness, and cost without considering the efficiency of template removal.

In several studies, template removal is performed through discontinued incubation in organic solvents or salt solutions. Unfortunately, complete template removal cannot be achieved even after extensive washing cycles, most probably because of poor solvent diffusion through pores within the polymer, highly cross-linked regions, or low solubility of the template in the removal solution.[17,18] In fact, protein permanence has been estimated to be nearly 25% of the initial template.[19] This has a negative impact on the analytical figures of merit of the sensing surface (*e.g.*, dynamic linear range, limit of detection (LOD), sensitivity, stability *etc.*).[20–22]

The development of ultrasensitive analytical detection methods for organophosphorus pesticides like dimethoate (DMT) plays a key role in healthy food production. DMT is an inhibitor of acetylcholinesterase (AChE), which can lead to the accumulation of acetylcholine and result in symptoms related to the autonomous and central nervous systems. The present study reports the electropolymerization of a polypyrrole-based MIP film for DMT detection, which is widely used as an organophosphorus pesticide. The proposed MIP-modified electrode detects DMT in the picomolar range (LOD of $(8 \pm 2) \times 10^{-12}$ M), which is five orders of magnitude lower than the limits set by EU legislation (*i.e.*, $\sim 40 \times 10^{-9}$ M).[23] Besides the electrochemical characterization of both MIP and non-imprinted polymer (NIP), complete removal of the template

[a]*Department of Chemistry, University of Bari Aldo Moro, Via E. Orabona 4, 70125 Bari, Italy. E-mail: paolo.bollella@uniba.it; nicoletta.ditaranto@uniba.it*

[b]*Centre for Colloid and Surface Science, University of Bari Aldo Moro, Via E. Orabona 4, 70125 Bari, Italy*

[c]*Department of Bioscience and Technology for Food, Agriculture and Environment, University of Teramo, Campus "Aurelio Saliceti" Via R. Balzarini 1, 64100 Teramo, Italy*

[d]*Dipartimento di Farmacia-Scienze del Farmaco, Università degli Studi di Bari Aldo Moro, 70125 Bari, Italy*

[e]*Faculty of Science and Engineering, Åbo Akademi University, 20500 Turku, Finland*

† Electronic supplementary information (ESI) available. See DOI: https://doi.org/10.1039/d2ay02024f

‡ These authors contributed equally to this work.

was achieved *via* alkaline washing (0.1 M NaOH for 45 min), as demonstrated from X-ray photoelectron spectroscopy (XPS) data.

Fig. 1a shows cyclic voltammograms (CVs) recorded in 0.01 M $Fe(CN)_6^{3-/4-}$ (in 0.05 M phosphate buffer containing 0.1 mM $NaNO_3$ as a supporting electrolyte; PB) before (naked gold electrode, black curve) and after the electrodeposition of PPy as NIP (red curve) and MIP (blue curve), using DMT as a templating molecule. The bare gold electrode reported an average anodic peak current (I_{pa}) of 452 ± 12 μA, which decreased for PPy-NIP (115 ± 8 μA) due to overoxidation occurring during the electrosynthesis (note that the polymerization was performed in the range between −0.4 and +1.5 V). This could be related to lower conductivity that hinders the faradaic reaction of $Fe(CN)_6^{3-/4-}$. Before the template removal, PPy-MIP exhibited a lower I_{pa} (46 ± 3 μA) than the bare gold electrode because of the templating molecules that inhibit the diffusion of the redox probe through the pores within the polymer.

Afterwards, the PPy-MIP electrodes were incubated in 0.1 M HCl solution for 45 min to remove the template. Fig. 1b shows CVs after electropolymerization (black curve) without any faradaic peak, which indicates complete surface coverage. After the acidic treatment (red curve), a couple of redox peaks for $Fe(CN)_6^{3-/4-}$ appeared with a midpoint potential ($E^{0\prime}$) of 0.296 ± 0.004 V. This could be ascribed to partial template removal facilitating the redox probe to access the electrode surface. The preparation procedure of MIP samples was repeated several times, showing considerable variability in the washing step for various imprinted polymers. To demonstrate the non-reproducibility of this washing protocol, CVs before and after HCl washing were recorded several times (for $n = 10$ samples). Contrary to what is shown in Fig. 1b, Fig. 1c shows only capacitive current before (black curve) and after (red curve) template removal. The latter could be ascribed to unsuccessful template removal and inaccessibility of the redox probe through the cavities. In addition, scanning electron microscopy (SEM) images of both PPy-MIP and PPy-NIP after HCl and NaOH template removal procedures are shown in Fig. S2.† For the HCl protocol, polymer swelling was noted, which might hinder successive analyte rebinding. The polymer swelling may be related to the protonation state of the polymer, which leads to progressive polymer denaturation. Conversely, in NaOH neither the MIP nor NIP layers underwent any uneven swelling phenomena.

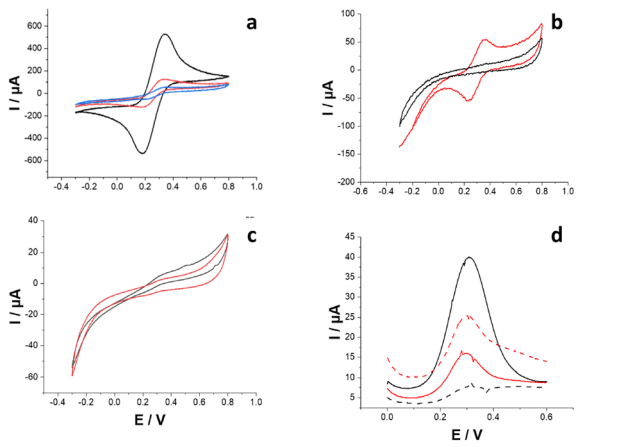

Fig. 1 (a) CVs of pure Au (black curve), NIP (red curve) and MIP (blue curve) after imprinting performed in 0.01 M $Fe(CN)_6^{3-/4-}$ in PB at a scan rate of 10 mV s^{-1}. (b and c) CVs of PPy-MIP after imprinting (black curve, samples I and II) and PPy-MIP after HCl washing (red curve, samples I and II) performed in 0.01 M $Fe(CN)_6^{3-/4-}$ in PB at a scan rate of 10 mV s^{-1}. (d) SWVs of the PPy-MIP electrode before (solid black curve) and after the first rebinding cycle using 100 × 10^{-12} M DMT (dashed black curve), compared with the second rebinding cycle at the same concentration of DMT before (solid red curve) and after rebinding (dashed red curve). SWVs were measured over a potential range between 0 and +0.6 V, frequency of 5 Hz and amplitude of 0.01 V in 0.01 M $Fe(CN)_6^{3-/4-}$ in PB.

Square wave voltammetry (SWV) analyses were performed to amplify the peak current related to indirect DMT sensing. The baseline voltammetry (Fig. 1d, black solid curve) showed a peak current of 40 μA, which dropped after performing the first rebinding in 100 × 10^{-12} M DMT solution (Fig. 1d, black dashed curve). The PPy-MIP was then treated again with HCl to remove the bound analyte. The SWV curve (Fig. 1d, red solid curve) shows a peak current of 25 μA lower than the starting baseline, proving the unsuccessful complete removal of the analyte from the MIP. Further rebinding, using the same concentration, led to an increase in the corresponding peak current, which proves a poor ability to remove DMT, most probably creating defects within the cavities, not allowing any further selective DMT rebinding.[15]

Additionally, PPy-NIP and PPy-MIP modified electrodes were characterized by XPS to evaluate the surface chemical composition of the electropolymerized films, before and after template removal protocol. All the wide scan spectra (Fig. S3†) show the presence of carbon, nitrogen and oxygen due to the polymer and gold, from the electrode on which the film was polymerized. On the surface of the PPy-MIP traces of sulfur and phosphorus were detected, characteristic elements of DMT.

The high-resolution XP spectral regions were then acquired, and the elemental surface atomic percentages were derived, as reported in Table S1.† In all cases, the percentage of carbon is the highest, as expected based on the composition of the film and the natural presence of surface contamination carbon, while the percentage of nitrogen is related to the structure of the polypyrrole (C/N ratio equal to 4, unless there is contamination). The presence of oxygen is also ascribable to the electropolymerization of pyrrole, which leads to the introduction into the structure of oxygenated species.[24] The presence of gold evidenced the formation of particularly thin films, with a thickness comparable to the maximum XPS sampling thickness (approximately 8–10 nm). Sulfur (quantitatively estimated) and phosphorus (qualitatively estimated) traces in the MIP, from the DMT, indicate that the template removal protocol was not able to quantitatively remove the templating molecules. N1s, C1s, and O1s XP spectra of the PPy-NIP electrode were curve-fitted (Fig. 2) to discriminate the different chemical environments (Table S2†). The N1s spectral region presents three components, at binding energies (BE) of 397.9 ± 0.2 eV,

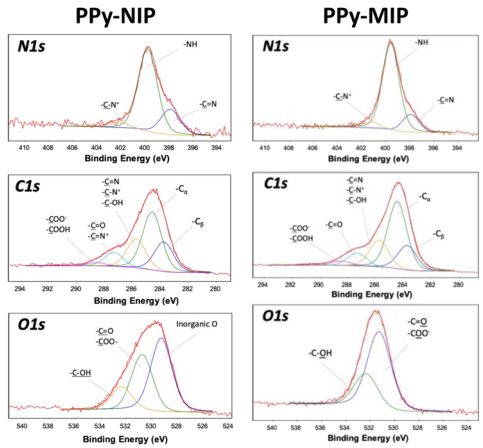

Fig. 2 Curve-fitted C1s, N1s, and O1s XPS spectra relative to a typical PPy-MIP sample.

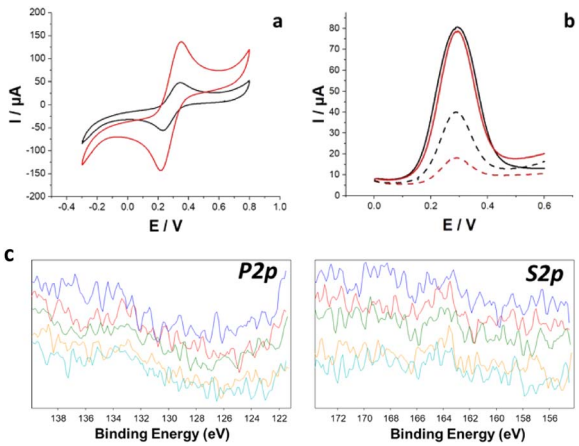

Fig. 3 (a) CVs of PPy-MIP before (black curve) and after (red curve) template removal with NaOH. CVs performed in 0.01 M $Fe(CN)_6^{3-/4-}$ PB at a scan rate of 10 mV s^{-1}. (b) SWVs of PPy-MIP electrode before (solid black curve) and after the rebinding cycle using 10 × 10^{-12} M DMT (dashed black curve) followed by the second rebinding cycle with 100 × 10^{-12} M DMT before (solid red curve) and after rebinding (dashed red curve). SWVs were performed over a potential range between 0 and +0.6 V, frequency of 5 Hz and amplitude of 0.01 V in 0.01 M $Fe(CN)_6^{3-/4-}$ in PB. SWVs were performed over a potential range between 0 and +0.6 V, frequency of 5 Hz and amplitude of 0.01 V in 0.01 M $Fe(CN)_6^{3-/4-}$ in PB. (c) S2p and P2p XP spectra relative to five replicate PPy-MIP samples washed with NaOH. A five-point Savitzky–Golay differentiation algorithm was applied to all the spectra to improve the signal-to-noise ratio.

399.7 ± 0.2 eV and 401.9 ± 0.2 eV, the assignments of which are shown in Table S2.† The relative abundances of the three components and the absence of the one related to C=N^+ (BE = 402.7 ± 0.2 eV) indicate the overoxidation of the polypyrrole, as expected from the potential values used for polymerization.[25]

The C1s region highlights the presence of five components with relative chemical assignments expected based on the polymer structure and its oxidized functionalities. Three components are present in the O1s region: two of them ascribable to the polymer structure (BE = 530.9 ± 0.2 eV and BE = 532.6 ± 0.2 eV) and one typical of oxygen in inorganic oxides (BE = 529.3 ± 0.2 eV). The latter can be associated with traces of aluminum, as a residue from the pyrrole synthesis process.

The carbon, nitrogen, and oxygen spectral regions of the PPy-MIP samples (Fig. 2, assignments reported in Table S3†) show a profile similar to those of the PPy-NIP ones, apart from the oxygen inorganic component, which probably arises due to the impurity removal during the extensive washing steps. The S2p spectral region was also investigated. It is possible to observe the presence of two doublets: one ascribable to –S=P (BE $S2p_{3/2}$ = 163.0 ± 0.2 eV) and the other typical of –S–P (BE $S2p_{3/2}$ = 167.3 ± 0.2 eV). These results confirmed what was already observed in the electrochemical characterization of the PPy-MIP films: the washing procedure and removal of the DMT analyte from the template proved not to be entirely effective and reproducible.

Considering the ineffectiveness of the acid washing, an alkaline washing procedure was adopted to modify the protonation state of the PPy film (0.1 M NaOH for 45 min under stirring). Fig. 3a shows CVs before (black curve) and after (red curve) the alkaline template removal procedure, evidencing its effectiveness with respect to the acidic washing, which is usually reported in the literature.[26] This could be ascribed to the reduced protonation of PPy and the repulsion of the negatively charged template. In concentrated alkaline solutions, the dedoping process should also be investigated. It has been reported that when a large amount of PPY is immersed in NaOH solutions, a deprotonation reaction takes place at the –NH moiety of pyrrole subunits, resulting in the elimination of dopant anions and a decrease in its conductivity.[27] In this case, the SWV curves revealed not only baseline reproducibility but also a good MIP response to the different DMT concentrations tested (Fig. 3b), notably in the picomolar range (detection of 10 × 10^{-12} and 100 × 10^{-12} M DMT for four rebinding/washing cycles with RSD < 3.7%, *data not shown*). The electrochemical results were further confirmed by XPS results.

Five replicated points were analyzed on two different PPy-MIPs, with no sulfur and phosphorus signals detected on PPy-

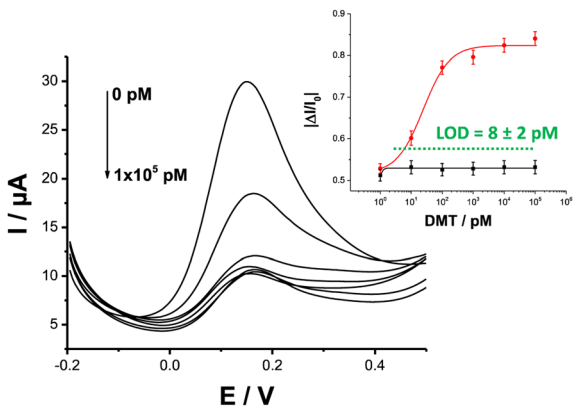

Fig. 4 SWVs of the PPy-MIP gold electrode at different DMT concentrations in the range between 1 × 10^{-12} M and 100 × 10^{-9} M. Inset: Calibration curve of the PPy-MIP (red curve) and PPy-NIP (negative control, black curve) electrodes between 1 × 10^{-12} M and 100 × 10^{-9} M of DMT.

MIP surfaces washed with 0.1 M NaOH (Fig. 3c). The high selectivity of the PPy-MIP platform was effectively proven by the almost zero response of the control assay (*i.e.*, PPy-NIP) in the whole concentration range. The limit of detection (LOD) was computed, being the concentration that leads to a response of $(\Delta I/I_0)$ mean $\pm k\sigma$, where $(\Delta I/I_0)$ mean is the average response of the blank sample, σ is the relative standard deviation, and k is a numerical factor chosen according to the level of confidence required ($k = 3$). The estimated LOD level corresponds to a DMT nominal concentration of $(8 \pm 2) \times 10^{-12}$ M, as shown in Fig. 4.

Conclusions

In conclusion, a PPy-MIP film for DMT detection was developed. Moreover, the successful template removal from the imprinted cavities was verified by comparing the XP spectra of imprinted and washed PPy-MIPs subjected to different template removal procedures. The most effective template removal was performed in 0.1 M NaOH (45 min under stirring). The developed sensor showed good sensitivity with a LOD of $(8 \pm 2) \times 10^{-12}$ M, which is five orders of magnitude lower than the limits set by EU regulation. These preliminary results prove the effectiveness of the alkaline washing procedure and the simple preparation of a PPy-MIP modified gold electrode that can be used to selectively detect DMT in real samples.

Author contributions

P. B., A. I. and N. D. wrote the manuscript. M. V., A. I. and A. T. performed all the measurements. P. B., N. D. and F. D. P. directly supervised M. V., A. I. and A. T. during the project. E. M., D. C. and L. T. revised the manuscript. The final version was approved by all authors.

Conflicts of interest

There are no conflicts to declare.

Acknowledgements

This work was supported by the PRIN project prot.2017RHX2E4 "At the forefront of Analytical ChemisTry: disrUptive detection technoLogies to improve food safety – ACTUaL". The following funding agencies are also acknowledged: the Academy of Finland projects #316881, #316883 "Spatiotemporal control of Cell Functions", #332106 "ProSiT—Protein Detection at the Single-Molecule Limit with a Self-powered Organic Transistor for HIV early diagnosis"; biosensori analitici usa-e getta a base di transistori organici auto-alimentati per la rivelazione di biomarcatori proteomici alla singola molecola per la diagnostica decentrata dell'HIV (6CDD3786); research for Innovation REFIN—Regione Puglia POR PUGLIA FESR-FSE 2014/2020; Dottorati innovativi con caratterizzazione industrial—PON R&I 2014–2020; "Sensore bio-elettronico usa-e-getta per l'HIV autoalimentato da una cella a combustibile biologica" (Bio-ElSens&Fuel); SiMBiT—Single molecule bio-electronic smart system array for clinical testing (grant agreement ID: 824946); PMGB—Sviluppo di piattaforme meccatroniche, genomiche e bioinformatiche per l'oncologia di precisione—ARS01_01195-PON "RICERCA E INNOVAZIONE" 2014–2020; Åbo Akademi University CoE "Bioelectronic activation of cell functions"; and CSGI are acknowledged for partial financial support.

References

1 J. J. BelBruno, *Chem. Rev.*, 2018, **119**, 94–119.
2 S. Ramanavicius, A. Jagminas and A. Ramanavicius, *Polymers*, 2021, **13**, 974.
3 N. Leibl, K. Haupt, C. Gonzato and L. Duma, *Chemosensors*, 2021, **9**, 123.
4 M. Lutfi Yola and N. Atar, *Curr. Anal. Chem.*, 2017, **13**, 13–17.
5 C. Karaman, O. Karaman, N. Atar and M. L. Yola, *Microchim. Acta*, 2022, **189**, 1–11.
6 Ö. S. Bölükbaşı, B. B. Yola, H. Boyacıoğlu and M. L. Yola, *Food Chem. Toxicol.*, 2022, **163**, 112994.
7 M. L. Yola, *Chemosphere*, 2022, **301**, 134766.
8 N. Özcan, H. Medetalibeyoglu, O. Akyıldırım, N. Atar and M. L. Yola, *Mater. Today Commun.*, 2020, **23**, 101097.
9 M. L. Yola and N. Atar, *J. Electrochem. Soc.*, 2018, **165**, H1.
10 F. Parnianchi, S. Kashanian, M. Nazari, C. Santoro, P. Bollella and K. Varmira, *Microchem. J.*, 2021, **168**, 106367.
11 H. Liu, P. Jin, F. Zhu, L. Nie and H. Qiu, *TrAC, Trends Anal. Chem.*, 2021, **134**, 116132.
12 N. Yuksel and S. Tektas, *J. Microencapsulation*, 2022, **39**, 176–196.
13 S. Bhakta and P. Mishra, *Sens. Actuators Rep.*, 2021, **3**, 100061.
14 E. Mazzotta, T. Di Giulio and C. Malitesta, *Anal. Bioanal. Chem.*, 2022, 1–36.
15 R. A. Lorenzo, A. M. Carro, C. Alvarez-Lorenzo and A. Concheiro, *Int. J. Mol. Sci.*, 2011, **12**, 4327–4347.
16 K. Farrington and F. Regan, *Talanta*, 2009, **78**, 653–659.
17 A. Ellwanger, C. Berggren, S. Bayoudh, C. Crecenzi, L. Karlsson, P. K. Owens, K. Ensing, P. Cormack, D. Sherrington and B. Sellergren, *Analyst*, 2001, **126**, 784–792.
18 B. S. Batlokwa, J. Mokgadi, T. Nyokong and N. Torto, *Chromatographia*, 2011, **73**, 589–593.
19 L. Levi and S. Srebnik, *J. Phys. Chem. B*, 2010, **114**, 107–114.
20 L. M. Gonçalves, *Curr. Opin. Electrochem.*, 2021, **25**, 100640.
21 B. Schweiger, J. Kim, Y. J. Kim and M. Ulbricht, *Sensors*, 2015, **15**, 4870–4889.
22 E. Mazzotta, S. Rella, A. Turco and C. Malitesta, *RSC Adv.*, 2015, **5**, 83164–83186.
23 COMMISSION REGULATION (EU) 2021/155 of 9 February 2021.
24 S. Sadki, P. Schottland, N. Brodie and G. Sabouraud, *Chem. Soc. Rev.*, 2000, **29**, 283–293.
25 C. Malitesta, I. Losito, L. Sabbatini and P. G. Zambonin, *J. Electron Spectrosc. Relat. Phenom.*, 1995, **76**, 629–634.
26 D. Capoferri, M. Del Carlo, N. Ntshongontshi, E. I. Iwuoha, M. Sergi, F. Di Ottavio and D. Compagnone, *Talanta*, 2017, **174**, 599–604.
27 Q. Xie, S. Kuwabata and H. Yoneyama, *J. Electroanal. Chem.*, 1997, **420**, 219–225.